Fluoromethacrylate-Containing Colloidal Dispersions: Phospholipid-Assisted Synthesis, Particle Morphology, and Temperature-Responsive Stratification

Anuradha Misra, William L. Jarrett, and Marek W. Urban*

School of Polymers and High Performance Materials, Shelby F. Thames Polymer Science Research Center, The University of Southern Mississippi, Hattiesburg, Mississippi 39406-0076

Received April 11, 2007; Revised Manuscript Received June 7, 2007

ABSTRACT: Because of unique properties of fluoropolymers, F-containing water dispersible colloidal dispersions continue to be of great interest and represent significant scientific challenges. These studies focus on the development and understanding of morphologies of F-containing colloidal particles synthesized in an aqueous phase in the presence of bioactive dispersing agents. When methyl methacrylate (MMA), *n*-butyl acrylate (*n*-BA), and heptadecafluorodecyl methacrylate (FMA) monomers are copolymerized in an aqueous phase, in the presence of phospholipids (PL), nonspherical particle morphologies are obtained. Their morphologies depend upon MMA/nBA ratios and lead to significantly different coalescence mechanisms and consequently surface properties. For higher MMA content, the particles are spherical, but at higher nBA contents, nonspherical morphologies are produced. This behavior is attributed to monomer starved conditions and the differences in reactivity ratios which forces copolymerization of FMA on the surface of *p*-MMA/*n*-BA particles, giving rise to nonspherical morphologies in the presence of biologically active PLs. Such prepared aqueous dispersions upon coalescence form films that exhibit ultralow static and kinetic coefficients of frictions which are attributed to internal phase stratification during coalescence.

Introduction

The attractiveness of fluoropolymers originates from their unique thermal, chemical, and mechanical stabilities and low surface energies. While these attributes make fluoropolymers particularly suitable candidates in biotechnology,[1] microelectronics, and other applications, processing temperatures and particularly film formation may be troublesome.[2−4] Further complexity arises from limited or no solubility of fluoromonomers in an aqueous phase. One approach to overcome these obstacles is to utilize colloidal copolymerization of fluoromonomers with other monomeric species to form stable colloidal particles capable of coalescence. Although several attempts have been made to prepare fluorinated colloidal dispersions, elaborate synthetic procedures and the use of cosolvents along with relatively low solids and fluorine contents represent significant challenges.[4−9] Another approach is to utilize a combination of dispersing agents during aqueous copolymerization of fluoro and acrylate families of monomers.[10−12] As recently shown,[10] the use of bioactive dispersing agents provides an opportunity for the synthesis of stable colloidal dispersions containing up to 15% w/w copolymerized F-monomers and, under monomer starvation conditions, *p*-methyl methacrylate/*n*-butyl acrylate/heptadeca fluorodecyl methacrylate (*p*-MMA/nBA/FMA) stable colloidal dispersions with unique nonspherical morphologies were obtained. It should be noted that without the use of bioactive dispersants only 8.5% w/w of a fluoropolymer was incorporated into pMMA/nBA. During the course of these studies, which primarily focused on synthetic aspects, it became quite apparent that understanding the mechanisms of the formation of nonspherical particle morphologies is essential to control particle morphologies and subsequently their film formation.[10] With this in mind, and considering the inherent complexity of F-containing colloidal dispersion synthesis, initial observations indicated that by varying MMA/nBA ratios while maintaining the same fluoro-acrylate (FMA) content composition, significant variations in particle morphologies were detected.

In view of these observations, one objective of these studies is to elucidate the origin of morphological changes in *p*-MMA/nBA/FMA particles, and to further advance limited knowledge of their coalescence. These issues are particularly relevant because previous studies showed that during film formation, phase separation between fluorinated and nonfluorinated components is observed for grafted fluorinated copolymers,[13,14] lattices with core−shell structures,[10−12,15,16] and blends of hydrogenated and fluorinated polymers.[4] Furthermore, F-containing components preferentially stratify near the film−air (F−A) interface, which results from unfavorable enthalpic interactions between fluoro and hydrocarbon polymer phases, leading to the reduction of the free energy driven by stratification of individual components.[17−20] Thus, stratification during coalescence is of particular interest which may be responsive to temperature changes and one example of fluoropolymer surfaces which exhibit temperature responses are fluoropolymer brushes.[21,22] Thus, another objective of this study is to determine how *p*-MMA/nBA/FMA particle morphologies affect thermoresponsive behavior during and after film formation.

Experimental Section

MMA, nBA, FMA, potassium persulfate (KPS), phosphoric acid bis(tridecafluorooctyl) ester ammonium salt (FSP), and sodium dodecyl sulfate (SDS) were purchased from Aldrich Chemical Co. 1,2-dilauroyl-*sn*-glycero-3-phosphocholine (DLPC) phospholipid was purchased from Avanti Polar Lipids, Inc. *p*-MMA/nBA/FMA dispersions were synthesized using a semicontinuous process outlined elsewhere[12,23] and adapted for small-scale polymerization. The reaction flask was placed in a water bath set at 78 °C, purged with N_2 gas, and charged with 20 mL of DDI water under continuous stirring at 300 rpm. SDS, FSP, and DLPC surfactants

* Author to whom all correspondence should be addressed.

10.1021/ma070852k CCC: $37.00
Published on Web 07/24/2007

Table 1. Composition and Particle Size Analysis of Colloidal Dispersions Containing 15%w/w of FMA with Different Ratios of MMA/nBA: (A) MMA/nBA (100:0); (B) MMA/nBA (90:10); (C) MMA/nBA (75:25); (D) MMA/nBA (50:50); (E) MMA/nBA (25:75); (F) MMA/nBA (10:90); (G) MMA/nBA (0:100)

composition	MMA/FMA	MMA/nBA/FMA	MMA/nBA/FMA	MMA/nBA/FMA	MMA/nBA/FMA	MMA/nBA/FMA	MMA/nBA/FMA
MMA/nBA ratio	100:0	90:10	75:25	50:50	25:75	10:90	0:100
individual components (w/w%)	A	B	C	D	E	F	G
DDI	59.5	59.5	59.5	59.5	59.5	59.5	59.5
methyl methacrylate	33.17	29.85	24.88	16.59	8.29	3.32	0
n-butyl acrylate	0	3.32	8.29	16.58	24.88	29.85	33.17
FMA	5.8	5.8	5.8	5.8	5.8	5.8	5.8
SDS	0.91	0.91	0.91	0.91	0.91	0.91	0.91
FSP	0.58	0.58	0.58	0.58	0.58	0.58	0.58
DLPC	0.05	0.05	0.05	0.05	0.05	0.05	0.05
$K_2S_2O_8$	0.23	0.23	0.23	0.23	0.23	0.23	0.23
solids (%)	40.5	40.5	40.5	40.5	40.5	40.5	40.5
particle size (nm)	95	106	120	140	146	150	160

were utilized, and Table 1 provides ratios of all dispersions prepared for the purpose of these studies. Surfactants were dissolved in water under continuous stirring at 600 rpm, followed by the addition of monomers to produce a semistable preemulsion. It should be noted that predispersions are monomer droplets dispersed in water which require continuous stirring in order to avoid monomer−water phase separation. For the seeded dispersion process, 10% (w/w) of the preemulsion and 18% (w/w) of the initiator solution were initially injected into the reaction kettle, thus facilitating the seed formation. The remaining predispersion was fed continuously without stirring over period of 4 h while the initiator solution was added for 4.5 h. Upon completion of the initiator feed, polymerization was allowed to continue for another 5 h. This process resulted in 40.5% w/w solids which was determined from the initial feed composition of the initiator monomer mixture and the analysis of the solid content after the synthesis. As listed in Table 1, the following compositions of colloidal particles containing 15% w/w of FMA were prepared: (A) MMA/nBA (100:0), (B) MMA/nBA (90:10), (C) MMA/nBA (75:25), (D) MMA/nBA (50:50), (E) MMA/nBA (25:75), (F) MMA/nBA (10:90), and (G) MMA/nBA (0:100).

Table 1 lists the particle size analysis with the accuracy of ± 5 nm obtained using a Microtrac UPA 250 instrument. Monomodal dispersions were obtained for all compositions listed in Table 1. Morphologies of colloidal particles were determined using a Zeiss EM 109-transmission electron microscope (TEM) in which colloidal dispersions were diluted to a 10 000:1 volume ratio (DDI:H_2O dispersions) and deposited on a Formvar coated copper TEM grid (Ted Pella, Inc.).

Colloidal particle solutions were allowed to coalesce for 72 h in a controlled environment at 23 °C temperature and 60% relative humidity (RH) to form approximately 10 μm thick films. The films were obtained by draw down on the polyvinyl chloride substrates (PVC). For contact angle measurements as well as atomic force microscopy (AFM) experiments colloidal solutions were coalesced on a glass slide using a draw bar to give an approximate film thickness of 10 μm. For thermoresponsive investigation, selected films were annealed at 60, 90, 120, and 150 °C for 2 h.

Solid-state ^{13}C NMR measurements were performed on a Varian ^{UNIT}YINOVA 400 spectrometer using a standard Chemagnetics 7.5 mm PENCIL-style probe. Samples were loaded into zirconia rotor sleeves, sealed with Teflon caps, and spun at a rate of 4.5 kHz. The standard cross-polarization magic angle spinning (CP/MAS) technique was used with high-power proton decoupling implemented during data acquisition. The acquisition parameters were as follows: The ^{1}H 90° pulse width was 4.0 μs, the cross-polarization contact time was 1 ms, the dead time delay was 6.4 μs, and the acquisition time was 45 ms.[24] A recycle delay of 3 s between scans was utilized. Experiments requiring simultaneous ^{1}H and ^{19}F decoupling were performed using a 3.2 mm HFXY probe. The ^{1}H and ^{19}F 90° pulse widths were 4.0 μs, the acquisition time was 26 ms, and the ^{19}F−^{13}C cross-polarization contact time was 10 ms. A recycle delay of 2 s and a samples spinning rate of 5 kHz were used.

Internal reflection infrared (IRIR) images were obtained using a Bio-Rad FTS 6000 Stingray system with a Ge internal reflection element (IRE). This system consists of a Bio-Rad FTS 6000 spectrometer, a UMA 500 microscope, an Image IR focal plane array (FPA) image detector, and a semispherical germanium IRE. IRIR images were collected using the following spectral acquisition parameters: under sampling ratio 4, step-scan speed 2.5 Hz, number of spectrometer steps 1777, number of images per step 64, and spectral resolution 8 cm^{-1}. The use of a Ge crystal in contact with the analyzed surface allows spatial resolution in the range of 1 μm.[25] In a typical experiment, spectral data set acquisition time was 17 min and image processing was performed using ENVI software (The Environment for Visualizing Images, Research Systems, Inc.) version 3.5.

Atomic force microscopy (AFM) measurements were conducted on a Nanoscope IIIa Dimension 3000 scanning probe microscope, Digital Instruments. A silicon probe with 125 μm long silicon cantilever, nominal force constant of 40 N/m and resonance frequency of 275 kHz were used in a tapping mode, allowing estimation of surface topography and roughness. Surface topography was determined on a 10 μm × 10 μm area with an image resolution of 256 × 256 pixels at a scan rate of 1 Hz. Surface roughness analysis was performed using Nanoscope version 5.30 r2 image analysis software. Surface tension measurements were obtained using a FTA200 dynamic contact angle analyzer, and a Qualitest 1055 friction tester was utilized to determine coefficients of friction.[26]

Results and Discussion

One of the objectives of these studies is to elucidate the origin of the formation of nonspherical morphologies obtained during the synthesis of *p*-MMA/nBA/FMA colloidal particles. During the first step, different nBA/MMA ratios containing the same amount of FMA (15% w/w) were synthesized, and Table 1 provides their compositions along with the particle size analysis. The particle size data indicate that for exactly the same polymerization conditions and % w/w solids, particle sizes varies from 95 to 160 nm. This increase parallels an increase of the nBA/MMA ratio. This behavior is attributed to lower density of *p*-nBA and the increased free volume of the *p*-nBA phase (T_g = −46 °C)[27] which, for the same molar amount of the monomer, result in the increased particle size. TEM images shown in Figure 1, A−G, illustrate morphologies of synthesized particles in the order of the increasing nBA/MMA ratio. As seen in Figure 1, A, spherical morphologies of *p*-MMA/FMA colloidal dispersions with no differences in electron density are observed. Similarly, for 90:10 and 75:25 MMA/nBA ratios, uniform morphologies are observed, as illustrated in Figure 1, images B and C, respectively. However, for 50:50 nBA/MMA ratio, nonspherical morphologies are produced and Figure 1, D illustrates TEM image of these particles. Similarly, as the nBA/MMA ratio increases (while maintaining the same FMA content), nonspherical morphologies prevail. This is illustrated in Figure 1, images E, F, and G, respectively.

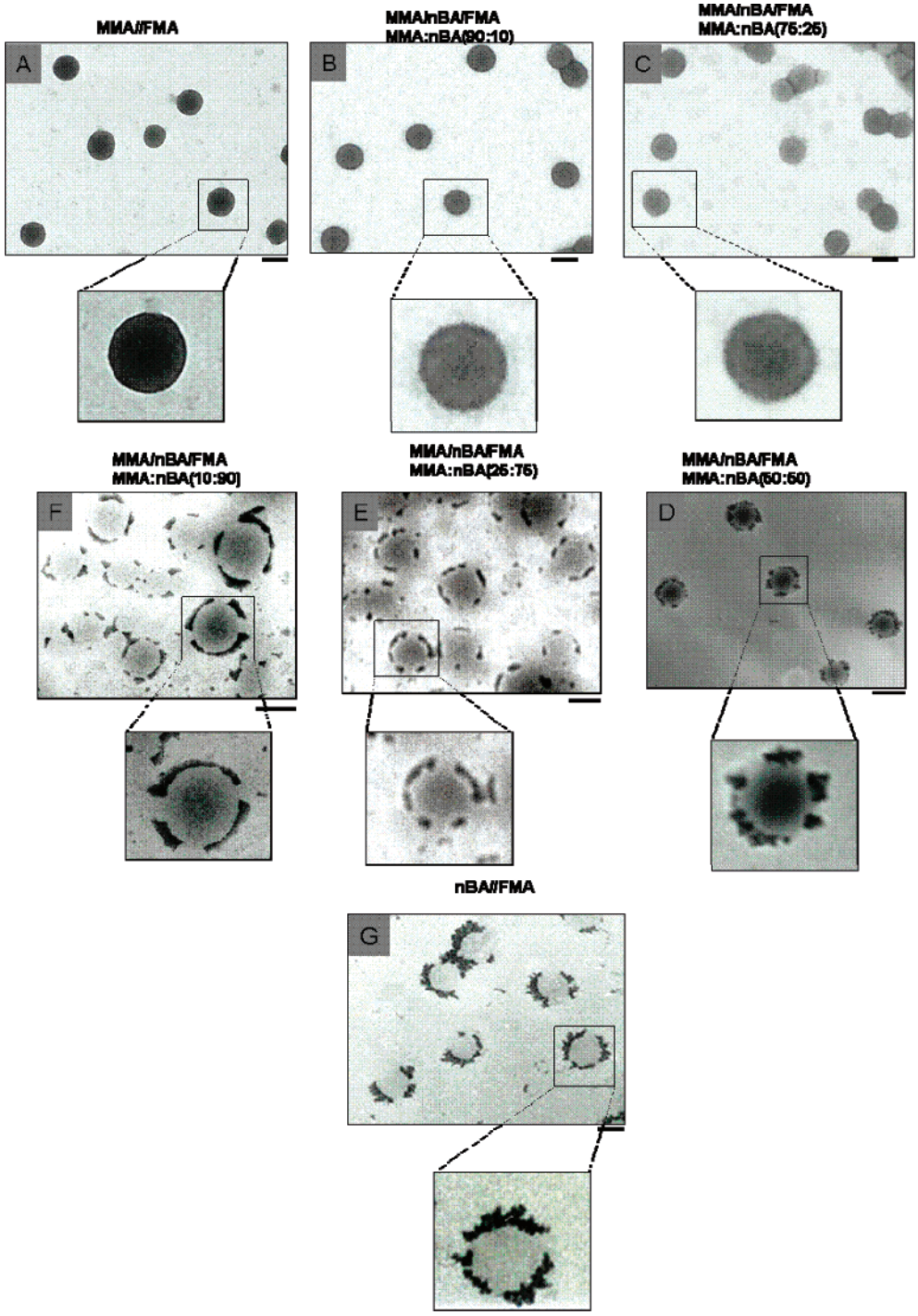

Figure 1. Transmission electron micrographs of colloidal particles containing 15%w/w of FMA with different MMA/nBA ratios: (A) MMA/nBA (100:0); (B) MMA/nBA (90:10); (C) MMA/nBA (75:25); (D) MMA/nBA (50:50); (E) MMA/nBA (25:75); (F) MMA/nBA (10:90); (G) MMA/nBA (0:100) (FMA to MMA/nBA ratio was maintained constant at 15:85 ratio).

Although TEM images shown in Figure 1 provide evidence that *p*-MMA/nBA/FMA particles exhibit nonspherical core−shell morphologies, in an effort to determine particle composition, solid-state NMR spectroscopy was utilized and films containing *p*-nBA/MMA/FMA (nBA/MMA ratio = 50:50) and *p*-MMA/FMA (ratio = 85:15) were analyzed. Figure 2, trace A, illustrates ^{13}C NMR spectrum of *p*-MMA/FMA and the presence of perfluoroalkyl side chain of FMA is detected at 115 ppm due to CF_2 groups of *p*-FMA.[12] In order to enhance selectivity of NMR analysis, we utilized cross-polarization of ^{19}F and ^{13}C along with the decoupling of ^{1}H and ^{19}F nuclei.[12] This technique facilitates through-space conditions, and the resulting spectrum provides information about functional groups in close proximity of the perfluoroalkyl side chains. For the purpose of these studies, experiments with the increasing cross-polarization contact times ranging from 2 to 10 ms were conducted. As shown in Figure 2, trace B, upon increasing cross-polarization contact time to 10 ms, only CF_2 and CF_3 groups are detected at 115 and 118 ppm, respectively. However, in *p*-MMA/FMA spectrum shown in Figure 2, trace B′, the CH_2 and C═O resonances at 50 and 180 ppm due to MMA are detected along with the 115 and 118 ppm peaks due to CF_2 groups.[28] Since this is a through space and not a bond-to-bond experiment, these data show that MMA units are in close proximity to FMA, thus indicating the formation of *p*-MMA/FMA random copolymer particles.

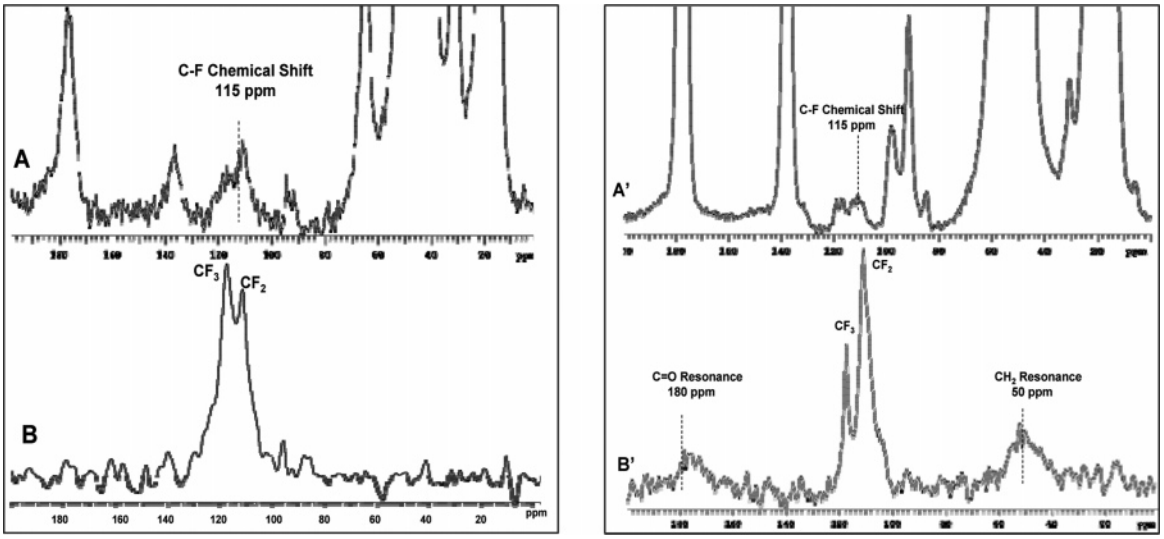

Figure 2. Solid-state NMR spectra of *p*-MMA/nBA/FMA copolymer films: (A) ^{13}C NMR spectrum; (B) ^{19}F and ^{13}C cross-polarization experiments with ^{1}H and ^{19}F decoupling; (A′) ^{13}C NMR spectrum; (B′) ^{19}F and ^{13}C cross-polarization spectrum obtained using ^{1}H and ^{19}F decoupling.

These experiments show that, under the same polymerization conditions, for higher MMA content, colloidal dispersions containing 15% FMA spherical morphologies are obtained. Also, *p*-MMA/FMA forms random copolymer under monomer starved conditions when both monomers are fed at the same time. However, the access of nBA (>50% w/w with respect to MMA) leads to the formation of nonspherical particles. If one considers the hydrophobicity of the employed monomers, it appears that nBA being more hydrophobic with respect to MMA,[27] should generate homogeneous particles in the presence of FMA. This is, however, not the case. FMA exhibits significantly higher hydrophobicity and oleophobicity with respect to nBA and MMA, and phase separates at higher nBA contents during polymerization. This behavior is attributed to the fact that during polymerization, MMA migrates to reactive sites and compositional drift in the growing particles occurs only when nBA/MMA ratios are equal or greater than 50:50. This behavior is attributed to higher reactivity ratios of MMA with respect to FMA (39), as compared to nBA, which is significantly smaller toward FMA (23).[29,33] As a result, when MMA and FMA are polymerized, random copolymers are obtained, whereas copolymerization of nBA/FMA results in block copolymers in which the *p*-FMA phase is present on the exterior of the particles, resulting in nonspherical morphologies.

The next question is what is the driving force for the growth of *p*-FMA phase on the surface of *p*-MMA/nBA seeds and what are the limiting factors that allow us to obtain stable dispersions containing up to 15% FMA solids. Because of higher and comparable reactivity ratios of MMA and FMA, spherical morphologies with no phase separation are produced, which is schematically shown in Scheme 1 A. For part B, *p*-nBA/FMA copolymer, *p*-FMA is locally polymerized on the *p*-nBA core, thus producing nonspherical morphologies. This was illustrated in Figure 1, images D−G. Furthermore, when MMA/nBA/FMA monomers are copolymerized, there is competition between nBA and FMA monomers for copolymerization with MMA and since FMA exhibits low aqueous solubility, it slowly migrates to reactive sites which is facilitated by the presence of PLs, thus allowing MMA-nBA to polymerize first, followed by FMA reactions on the existing *p*-MMA/nBA core. As a consequence, nonspherical core−shell are obtained for the nBA higher content. It should be noted that the particle size measurements during polymerization revealed monomodal particle size distribution at all stages, thus showing that pFMA phase does not polymerize as a separate entity.

Although one may argue that *Q* and *e* values of TFE should not be used to access the reactivity of FMA, which is a valid point, there is no literature data available on fluoroacrylates. However, taking into account the solubility of each monomer in an aqueous phase in the presence of other monomers, and considering the order of reactivity being MMA > nBA ≫ FMA and polarity of each monomer, the following scenario may be considered: FMA is more miscible in more polar MMA, but less miscible within nBA, and therefore spherical particles are formed for pMMA/FMA, whereas nonspherical particles are obtained for *p*-nBA/FMA polymerizations. Although solubility and polarity indeed contribute to the sequence of events leading to the formation of nonspherical particles, the reactivity of each monomer, and the lowering of the surface tension facilitated by PL dominate the polymerization process.

The limiting factor for FMA incorporation into colloidal dispersions is the stability of colloidal particles. In these studies we utilized bioactive PLs, which form random mixed micellar structures with SDS and FSP surfactants. PLs, being the main constituents of the cell membranes, serve as selective barriers for bioactive species as well as provide support for membrane protein transport.[30] When PLs along with SDS and FSP form mixed micellar structures, the *p*-FMA phase growth on the *p*-MMA/nBA colloidal particles is facilitated due to the reduction of the overall surface tension of the aqueous phase from 72 to about 1−5 mN/m.[31,32] This is the reason for choosing DLPC as one of the dispersing agents during synthesis in order to form *p*-MMA/nBA seeds, followed by creating monomer starvation conditions, which force FMA monomers to migrate to reactive sites. Although the exact mechanism of PL's needs further examination, one can envision that DLPC may form bilayered structures with hydrophobic interior and hydrophilic exterior, thus facilitating transport of FMA monomers to already formed *p*-MMA/nBA seeds. In essence, PLs exhibit dual functions: (1) they facilitate transport of FMA to the *p*-MMA/nBA core and (2) they stabilize the growing particles. A schematic diagram illustrating formation of *p*-MMA/FMA (A), nBA/FMA (B), and *p*-MMA/nBA/FMA (C) colloidal dispersions with different particle morphologies are illustrated in Scheme 1.

Scheme 1. Schematic Diagram Illustrating the Effect of Monomer Copolymerization on Particle Surface Morphology

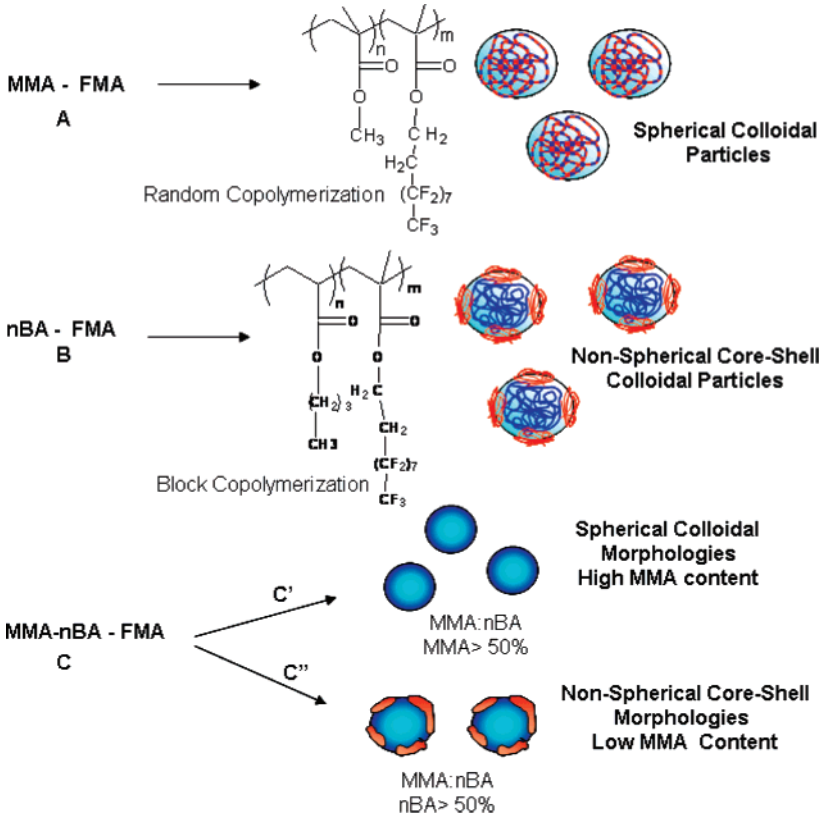

Another objective of this study is to create polymeric films which coalesce under ambient condition and exhibit fluoropolymer properties. In the context of the formation of nonspherical particle morphologies, the next question is how the presence of the FMA phase on *p*-MMA/nBA particles will affect coalescence. For that reason colloidal dispersions of *p*-nBA/FMA and *p*-MMA/FMA were allowed to coalesce, and their surfaces were analyzed using IRIRI which allows us to spatially resolve chemical surface heterogeneities with 1 μm spatial resolution. Analysis of the C−O−C stretching modes due to *p*-MMA and *p*-nBA at 1165 and 1145 cm^{-1} as well as C−F stretching bands at 1203 cm^{-1} due to FMA are of particular interest because these bands allow us to follow the mobility of fluorinated species within the film. The choice of the C−F stretching mode at 1203 cm^{-1} for monitoring pFMA distribution on the surface over the C−O−C stretching at 1145 cm^{-1} was dictated by the C−O−C overlap with the same C−O−C vibrations in pMMA. Figure 3 illustrates an IRIR image of the films obtained from *p*-nBA/FMA colloidal particles which was obtained by tuning into the 1203 cm^{-1} band due to FMA. Analysis of the image shown in Figure 3A indicates that the distribution of the *p*-FMA phase is heterogeneous. The corresponding IR spectra recorded from areas 1 and 2 show that the 1203 cm^{-1} band is absent in area 1 (Figure 3B, trace a), but detected in the area 2 (Figure 3B, trace b), thus showing the presence of *p*-FMA in the red region (area 2) of image A. For reference purposes, trace c illustrates the IR spectrum of FMA monomer. These data show that during coalescence of *p*-FMA component, which is present on the exterior of the colloidal particles, the *p*-FMA phase separates out from *p*-nBA, thus leading to vertically stratified films. Previous studies have shown that, for the films coalesced from *p*-MMA/nBA/FMA (15% w/w FMA) dispersions, two distinct phases of *p*-FMA and *p*-MMA/nBA are formed.[10]

Similar analysis of the films containing *p*-MMA/FMA was conducted by tuning into the 1203 cm^{-1} band due to FMA and the 1145 cm^{-1} band due to MMA. This is illustrated in Figure 4, parts A and B. In contrast to *p*-nBA/FMA, no compositional variations exist and no phase separation occurs, as indicated by the corresponding IR spectrum recorded from areas 1 and 2. These data are in agreement with the results of TEM and NMR analysis. It is apparent that the heterogeneity during film formation is influenced by acrylate components of colloidal dispersions and their mobility during and after coalescence. In the case of *p*-nBA/FMA, due to the low T_g of *p*-nBA phase (−46 °C),[27] the minimum film formation temperature (MFFT) is significantly lower which facilitates mobility during film formation, and thus ability of the *p*-FMA phase to diffuse to the F−A interface driven by its low surface energy. In contrast, for *p*-MMA/FMA with the T_g of *p*-MMA and *p*-FMA of 100 and 175 °C, respectively, film formation is inhibited.

In order to facilitate coalescence under ambient conditions,[12,27] *p*-MMA/FMA and *p*-nBA/FMA dispersions were mixed in equal amounts and allowed to coalesce, followed by measurements of the static and kinetic coefficients of friction. The values of 0.145 and 0.042, respectively, were obtained, which are significantly smaller than for *p*-MMA/nBA films (0.78 and 0.38). Although only 15% w/w of fluoropolymer with respect to MMA/nBA ratio was incorporated, the changes of surface properties are drastic. This is attributed to stratification of the *p*-FMA phase to the F−A interface, leading to surface enrichment resulting from stratification of low surface energy *p*-FMA phase. As shown by the previous studies,[10] *p*-FMA forms network structure during coalescence and due to low surface energy, migrates to the F−A interface.

It is well-established that temperature significantly affects phase separation in polymeric films. In order to determine the effect of temperature on the degree of stratification of the

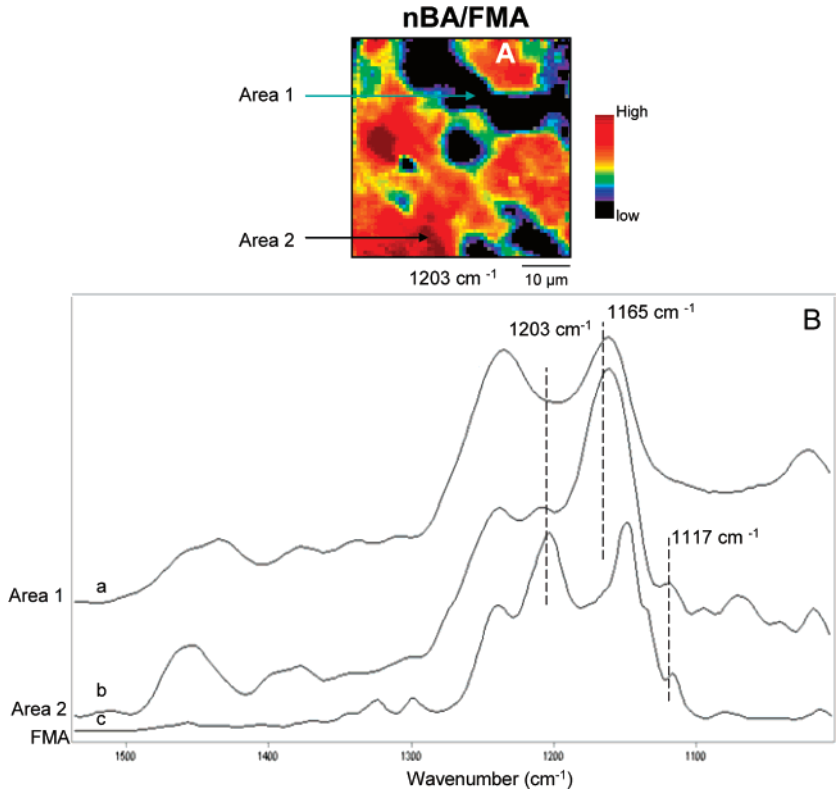

Figure 3. IRIR images recorded from the F−A interface of coalesced films obtained from *p*-nBA/FMA colloidal dispersions: (A) image obtained by tuning into 1203 cm^{-1}; (B) IR spectra recorded from areas labeled 1 and 2 in image A; (a) IR spectrum of area 1; (b) IR spectrum of area 2; (c) IR spectrum of FMA.

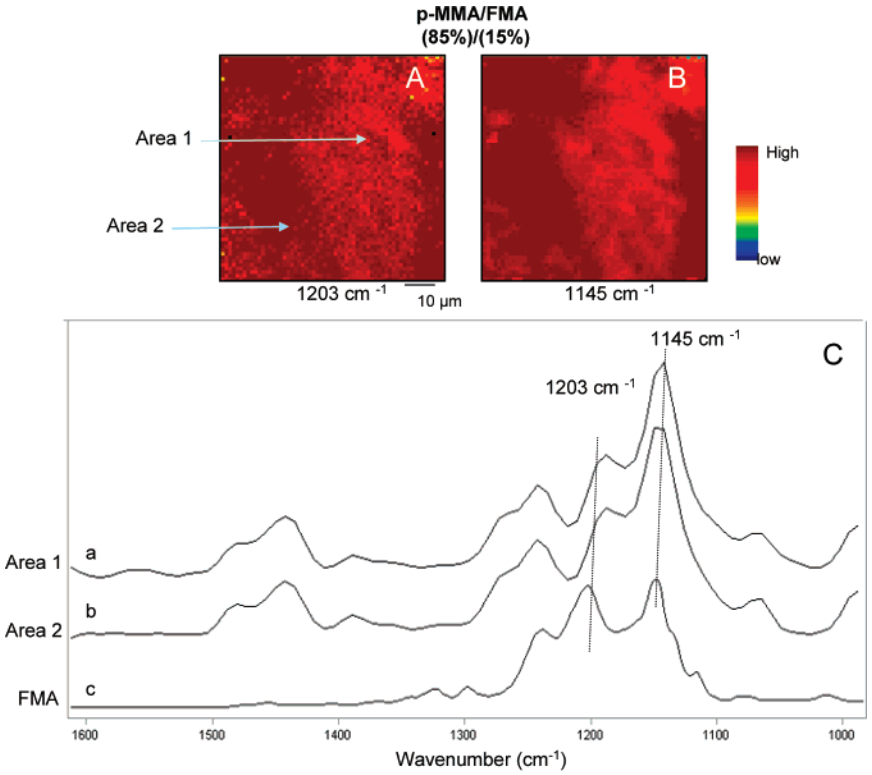

Figure 4. IRIR images recorded from the F−A interface of coalesced films obtained from *p*-MMA/FMA colloidal dispersions: (A) image obtained by tuning into 1203 cm^{-1}; (B) image obtained by tuning into 1145 cm^{-1}; (C) IR spectra recorded from areas labeled 1 and 2 in image A; (a) IR spectrum of area 1; (b) IR spectrum of area 2; (c) IR spectrum of FMA.

p-FMA phase in *p*-MMA/FMA and *p*-nBA/FMA mixture, films containing 15% w/w FMA were annealed at 60, 90, 120, and 150 °C and AFM measurements were conducted. The results are shown in Figure 5, where AFM images A−D illustrate a series of phase and height images recorded from the F−A interface of the films coalesced at 23 °C (A/A′), annealed at 60 (B/B′), 120 (C/C′), and 150 °C (D/D′). The root-mean-square roughness (rms) of height deviations taken from the mean data

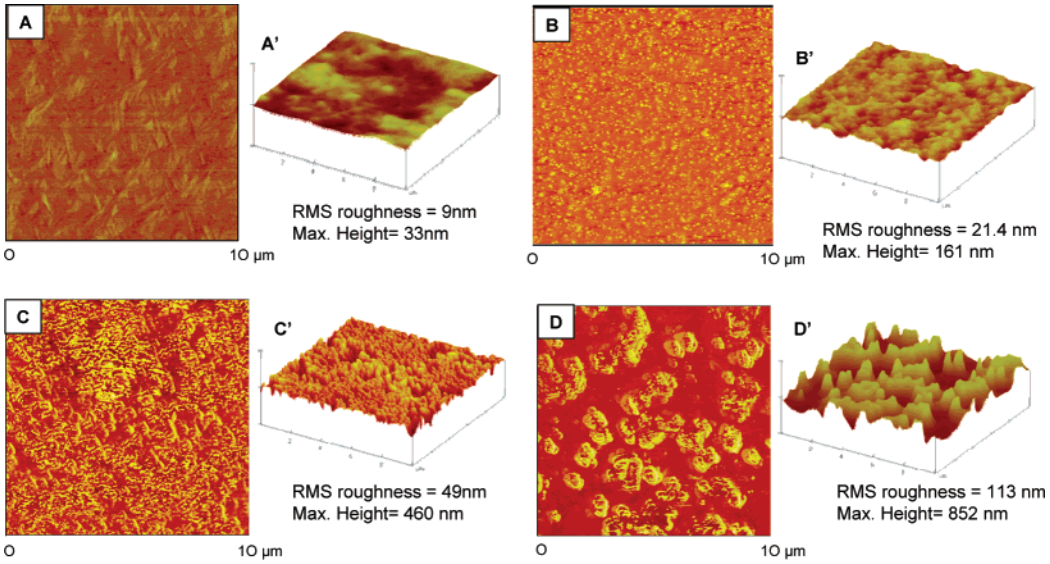

Figure 5. AFM phase (A) and AFM 3-D (A′) images of polymeric films coalesced from *p*-MMA/FMA and *p*-nBA/FMA 50:50 colloidal mixture coalesced at 23 °C. Images B/B′, C/C′, and D/D′ were obtained from the same films annealed at 60, 120, and 150 °C, respectively.

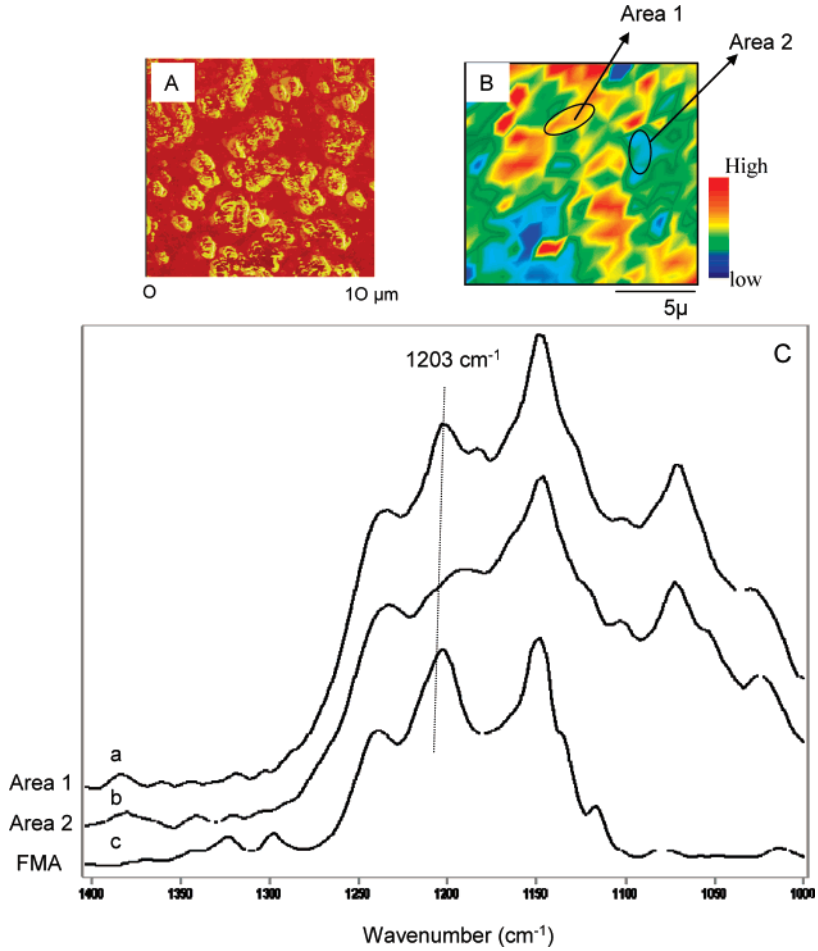

Figure 6. IRIR images recorded from the F−A interface of coalesced films obtained from *p*-MMA/FMA and *p*-nBA/FMA colloidal dispersion mixture (50:50) after annealing at 150 °C: (A) AFM phase image; (B) image obtained by tuning into 1203 cm $^{-1}$ band; (C) IR spectra recorded from areas labeled 1 and 2 in image B; (a) IR spectrum of area 1; (b) IR spectrum of area 2; (c) IR spectrum of FMA.

plane is shown in Figure 5, image A, and illustrates two phase components attributed to fluorinated (brighter regions) and nonfluorinated phases (darker regions). Upon annealing at 60 °C, small domains begin to appear, and at 120 and 150 °C, phase separation becomes prominent, where the increase of the domain size is observed. This is also reflected in the rms roughness values which increase as a function of temperature.

In order to confirm that indeed upon annealing the fluoropolymer is responsible for the formation of surface domains IRIRI measurements were conducted. While Figure 6A illustrates an AFM phase image of the film annealed at 150 °C, Figure 6B represents IRIR image of the 1203 cm^{-1} band due to C−F stretching vibrations of *p*-FMA. As seen, distribution of the *p*-FMA phase is heterogeneous with red areas corre-

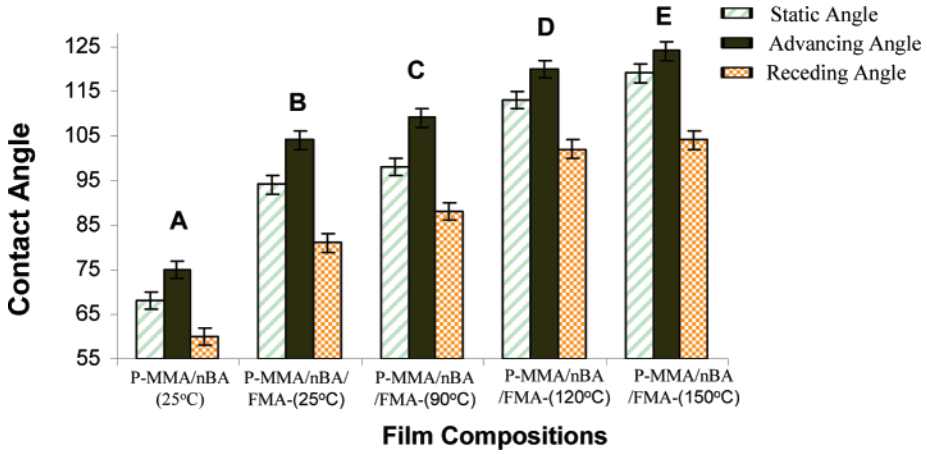

Figure 7. Contact angle measurements (water) for (A) *p*-MMA/nBA (25 °C), (B) *p*-MMA/nBA/FMA (15% w/w) (25 °C), and *p*-MMA/nBA/FMA films annealed at (C) 90 °C, (D) 120 °C, and (E) 150 °C.

Scheme 2. Schematic Diagram Illustrating the Effect of Temperature on Surface Roughness

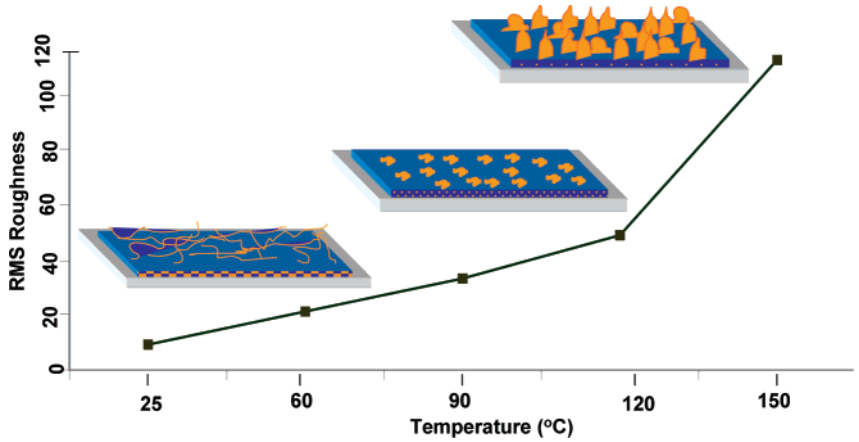

sponding to elevated *p*-FMA phase. Furthermore, analysis of areas 1 and 2 indicate that area 1 exhibits enhanced intensities of the 1203 cm^{-1} band, thus signifying the presence of the *p*-FMA rich domains and reduced intensities in area 2. These changes correspond to the phase image data shown in Figure 6A. Furthermore, these features are also responsible for the increase of the contact angle. As illustrated in Figure 7, static, advancing, and receeding water contact angle measurements show that static and advancing contact angles increase to 118 and 124°, respectively, upon annealing at 150 °C. In summary, temperature has a significant effect on stratification not only of low molecular weight species, but also on high molecular weight polymers such as *p*-FMA phase in *p*-MMA/nBA/FMA SYSTEM. Scheme 2 illustrates a schematic diagram depicting the effect of temperature on surface roughness.

Conclusions

Colloidal dispersions *p*-MMA/nBA/FMA containing 15% w/w FMA and various nBA/MMA ratios were synthesized using a combination of SDS/FSP/DLPC dispersing agents under monomer starved conditions. The formation of stable F-containing particles is attributed to the presence of bioactive DLPC phospholipids and monomer starvation conditions during polymerization. These studies also showed that when nBA/MMA ratio is greater than 1:1, FMA polymerizes on the surface of *p*-MMA/nBA, and nonspherical particles of *p*-MMA/nBA/FMA are formed. In order to facilitate film formation *p*-MMA/FMA particles and *p*-nBA/FMA phases were mixed which upon coalescence forms stratified films and the degree of *p*-FMA stratification toward the F-A interface depends on temperature. As a result, a number of surface properties such as surface roughness and contact angle or surface energy can be altered.

Acknowledgment. This work was supported primarily by the MRSEC Program of the National Science Foundation under Award No. DMR 0213883. The authors also acknowledge use of instrumentation and facilities through the Materials Research Facilities Network (MRFN) supported by the NSF MRSEC program (DMR 0213883) as well as Major Research Instrumentation program DMR 0215873.

References and Notes

(1) Wang, J.; Mao, G.; Ober, C. K.; Kramer, E. J. *Macromolecules* **1997**, *30*, 1906.
(2) Milner, S. T. *Science* **1991**, *251*, 905.
(3) Lednev, I. K.; Karnoup, A. S.; Sparrow, M. C.; Asher, S. A. *J. Am. Chem. Soc.* **1998**, *120*, 6518.
(4) Linemann, R. F.; Malner, T. E.; Brandsch, R.; Bar, G.; Ritter, W.; Mulhaupt, R. *Macromolecules* **1999**, *32*, 1715.
(5) Koendrick, G. H.; Sacanna, S.; Pathmamanoharan, C.; Rasa, M.; Philipse, A. P. *Langmuir* **2001**, *17*, 6086.
(6) Sacanna, S.; Koenderink, G. H.; Philipse, A. P. *Langmuir* **2004**, *20*, 8398.
(7) Ha, J.; Park, I.; Lee, S.; Kim, D. *Macromolecules* **2002**, *35*, 6811.
(8) Thomas, R. R.; Lloyd, K. G.; Stika, L. M.; Stephens, L. E.; Megallanes, G. S.; Dimonie, V. L.; Sudol, E. D.; El-Aasser, M. S. *Macromolecules* **2000**, *33*, 8828.
(9) Landfester, K.; Rothe, R.; Antonietti, M. *Macromolecules* **2002**, *35*, 1658.
(10) Singh, A.; Dreher, W. R.; Urban, M. W. *Langmuir* **2006**, *22*, 524.
(11) Dreher, W. R.; Singh, A.; Urban, M. W. *Macromolecules* **2005**, *38*, 4666.

(12) Dreher, W. R.; Jarrett, W. L.; Urban, M. W. *Macromolecules* **2005**, *38*, 2205.
(13) Mawson, S.; Johnston, K. P.; Betts, D. E.; MaClain, J. B.; Desimone, J. M. *Macromolecules* **1997**, *30*, 71.
(14) Park, I.; Lee, S. B.; Choi, C. K. *Macromolecules* **1998**, *31*, 75553.
(15) Marion, P. B.; Juhue, D.; Lang, J. *Macromolecules* **1997**, *30*, 123.
(16) Chen, Y.; Ying, L.; Yu, W. J.; Kang, E.; Neoh, K. *Macromolecules* **2003**, *36*, 9451.
(17) Li, K.; Wu, P.; Han, Z. *Polymer* **2002**, *43*, 4079.
(18) Kassis, C. M.; Steehler, J. K.; Betts, D. E.; Guan, Z.; Romack, T. J.; DeSimone, J. M.; Linton, R. W. *Macromolecules* **1996**, *29*, 3247.
(19) Krupers, M.; Möller, M. *Macromol. Chem. Phys.* **1997**, *198*, 2163.
(20) McCloskey, C. B.; Yip, C. M.; Santerre, J. P. *Macromolecules* **2002**, *35*, 924.
(21) Granville, A. M.; Boyes, S. G.; Akgun, B.; Foster, M. D.; Brittain, W. J. *Macromolecules* **2004**, *37*, 2790.
(22) Granville, A. M.; Boyes, S. G.; Akgun, B.; Foster, M. D.; Brittain, W. J. *Macromolecules* **2005**, *38*, 3263.
(23) Davis, S. D.; Hadgraft, J.; Palin, K. J. *Encyclopedia of Emulsion Technology*; Marcel Dekker: New York, 1985; Vol. 2.
(24) Schaefer, J.; Stejskal, E. O.; Buchdahl, R. *Macromolecules* **1977**, *10*, 384.
(25) Otts, D.; Zhang, P.; Urban, M. W. *Langmuir* **2002**, *18*, 6473.
(26) *ASTM Standard Test D 1894−01*.
(27) Lestage, D. J.; Urban, M. W. *Langmuir* **2004**, *20*, 6443.
(28) Liu, S. F.; Schmidt-Rohr, K. *Macromolecules* **2001**, *34*, 8416.
(29) Odian, G. *Principles of Polymerization*; John Wiley & Sons: New York, 2004.
(30) Voet, D.; Voet, J. G. *Biochemistry*, 1st ed.; Wiley & Sons, Inc.: New York, 1995.
(31) Nii, T.; Ishii, F. *Colloids Surf.* **2004**, *39*, 57.
(32) Pinazo, A.; Wen, X.; Liao, Y. C.; Prosser, A. J.; Franses, E. I. *Langmuir* **2002**, *18*, 8888.
(33) Since no *Q* and *e* values for FMA are available in the literature, the reactivity ratios were estimated by utilizing *Q* and *e* values for MMA, nBA, and tetrafluoroethylene (TFE).

MA070852K